CHEMISTRY OF MATERIALS

pubs.acs.org/cm

Perspective

Unveiling the Liquid Electrolyte Solvation Structure by Small Angle X-ray Scattering

Xinyi Liu, Lingzhe Fang, Xingyi Lyu, Randall E. Winans, and Tao Li*

Cite This: *Chem. Mater.* 2023, 35, 9821−9832

Read Online

ACCESS | Metrics & More | Article Recommendations

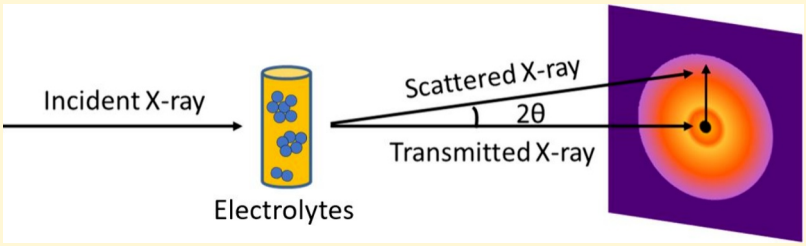

ABSTRACT: The fundamental understanding of the liquid electrolyte (LE) solvation structure and electrode−electrolyte interface behavior will bring more in-depth thinking and revolutionary changes to the entire electrochemical energy storage field. Regardless of the variety of techniques available, the methods employed to investigate electrolyte solvation structures over a long-range are severely limited. Small-angle X-ray scattering (SAXS) is an ideal complement to Raman spectroscopy, Fourier transform infrared spectroscopy, or nuclear magnetic resonance, which offers a unique perspective from a larger scale on clusters or networks in electrolytes. Understanding the solvation structures from a few angstroms to hundreds of nanometers will undoubtedly lay a good foundation for studying the macroscopic transport properties, such as viscosity and ionic conductivity, of the LEs. In this Perspective, we discuss the use of SAXS to investigate the solvation structures in different electrolyte systems, a prospect for the SAXS broader application in the electrolyte study, and some challenges that need to be solved in the SAXS application.

INTRODUCTION

The transition from fossil energy to sustainable energy strongly relies on the development of efficient energy storage technologies. Among the various energy storage technologies, electrochemical energy storage such as rechargeable batteries, supercapacitors, and fuel cells have received tremendous research interest.[1−10] As an important component of batteries, the electrolyte mainly transfers ions and blocks electrons. In the electrochemical energy storage devices that have been successfully commercialized, liquid electrolytes (LEs) still occupy the majority market share.[11,12] However, the LE investigation is still challenging because of its amorphous structure and fast dynamics. More importantly, it is difficult to establish relationships between the molecular scale electrolyte kinetics with macroscopic physical properties[13] (viscosity, ionic conductivity, transference numbers, etc.) and expand further to the electrochemical performances such as power density, cycle life, rate capability, extreme working condition performances, and safety.[14,15]

Due to the repulsive and attractive forces of interactions between adjacent ions and molecules, short-range order exists, which is known as solvation structures.[16] The study of the solvation structure is the cornerstone of all subsequent research on the LEs. According to previous research, the LE solvation structures may exist at multiple length scales, from a few angstroms to hundreds of nanometers.[17−23] The microscopic structure of different LEs has been investigated via different spectroscopic techniques, such as Fourier transform infrared (FTIR) spectroscopy,[21,24,25] Raman spectroscopy,[26−30] nuclear magnetic resonance (NMR),[31,32] and neutron scattering.[17,20] However, these techniques are only sensitive to the local molecular bonds and orientations, which are the local short-range information (below 1 nm), and it is challenging to capture the information on the middle-range length scale (1−10 nm) and long-range length scale (above 10 nm). Some studies have raised the possibility that the LEs is heterogeneous and indicate that the domains of cation/anion, anion, or solvent exist.[17−23] This means that it is no longer possible to fully characterize the LEs by FTIR, Raman, or NMR techniques. If the LEs system is heterogeneous, then it will exhibit nanoscale density variation. And small-angle X-ray scattering (SAXS) is a technique that uses nanoscale electron density variation to characterize samples. The SAXS method

Received: July 1, 2023
Revised: November 7, 2023
Accepted: November 7, 2023
Published: December 1, 2023

Scheme 1. Schematic of Synchrotron SAXS Measurement

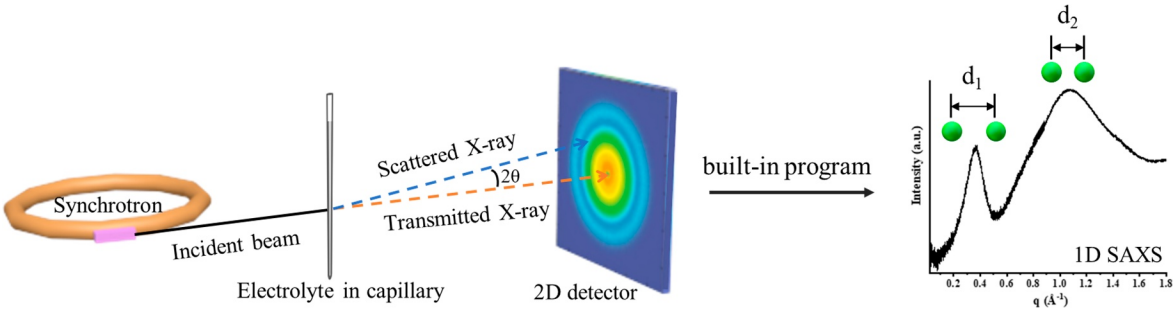

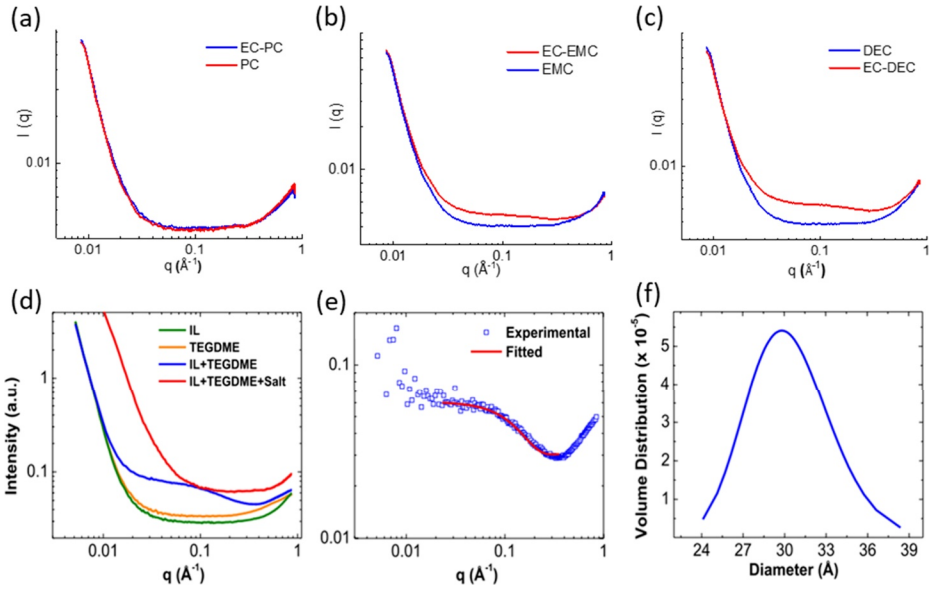

Figure 1. SAXS data of (a) EC/PC (1/9) and PC, (b) EC/EMC (1/9) and EMC, and (c) EC/DEC (1/9) and DEC. (d) SAXS data of IL, TEGDME, IL/TEGDME, and IL/TEGDME/Salt systems. (e) Fitted curve of subtracted data of the capillary from the IL/TEGDME solution. (f) Size distribution obtained after fitting the spherical model on the subtraction result of (e). Figure reproduced with permission from ref 37. Copyright 2021 Elsevier.

studies the materials at large distances or small angles, which can probe the intermolecular spacing, cluster size, or inhomogeneity domains from 1 to 150 nm.[33]

Herein we intend to show how SAXS is uniquely positioned to study LE systems in their native environment. We begin with a discussion of the application of SAXS in the study of conventional electrolytes with a lower salt concentration, which is composed of lithium hexafluorophosphate ($LiPF_6$) and organic solvents ethyl carbonate (EC), propylene carbonate (PC), dimethyl carbonate (DMC), ethyl methyl carbonate (EMC), and diethyl carbonate (DEC). However, because of the safety issue of traditional organic electrolytes, nonvolatile, nonflammable aqueous electrolytes have become promising alternative electrolytes. High concentration "water-in-salt" (WIS) electrolytes with excellent electrochemical and physical properties are proposed. Combining SAXS and molecular dynamics (MD) simulation, the solvation structures and dynamics of WIS electrolytes are investigated, and the discussion extends to the "solvent-in-salt" electrolytes. Finally, we will discuss the unique advantages of using in situ SAXS and GISAXS in the liquid study and some challenges that need to be solved for future use.

WORKING PRINCIPLES OF SAXS

The schematic representation of the synchrotron SAXS measurement is depicted in Scheme 1. In this setup, incident X-rays traverse the sample, and the resulting scattering signal is captured by a two-dimensional (2D) detector. The recorded 2D image can subsequently be transformed into a one-dimensional (1D) SAXS curve. The relationship between the scattering angle 2θ and the scattering vector q is expressed as $q = 4\pi \sin(\theta)/\lambda$, where λ denotes the wavelength of the X-rays.

Typically, SAXS spectra exhibit the form factor of the examined samples. However, when sample concentrations increase or specific interactions occur within the sample, the structure factor becomes discernible. This phenomenon is visually represented by peaks emerging, as depicted in Scheme 1. The respective interparticle distances or d-spacings of these peaks within the 1D SAXS spectra can be determined using the formula $d = 2\pi/q$. Notably, this implies that lower q values correspond to larger d-spacings of the nanostructure under scrutiny.

CONVENTIONAL ELECTROLYTES

Organic solvents, salts, and additives typically constitute commercial liquid electrolytes. Usually, organic solvents combine two or three components, which can be roughly

https://doi.org/10.1021/acs.chemmater.3c01648
Chem. Mater. 2023, 35, 9821−9832

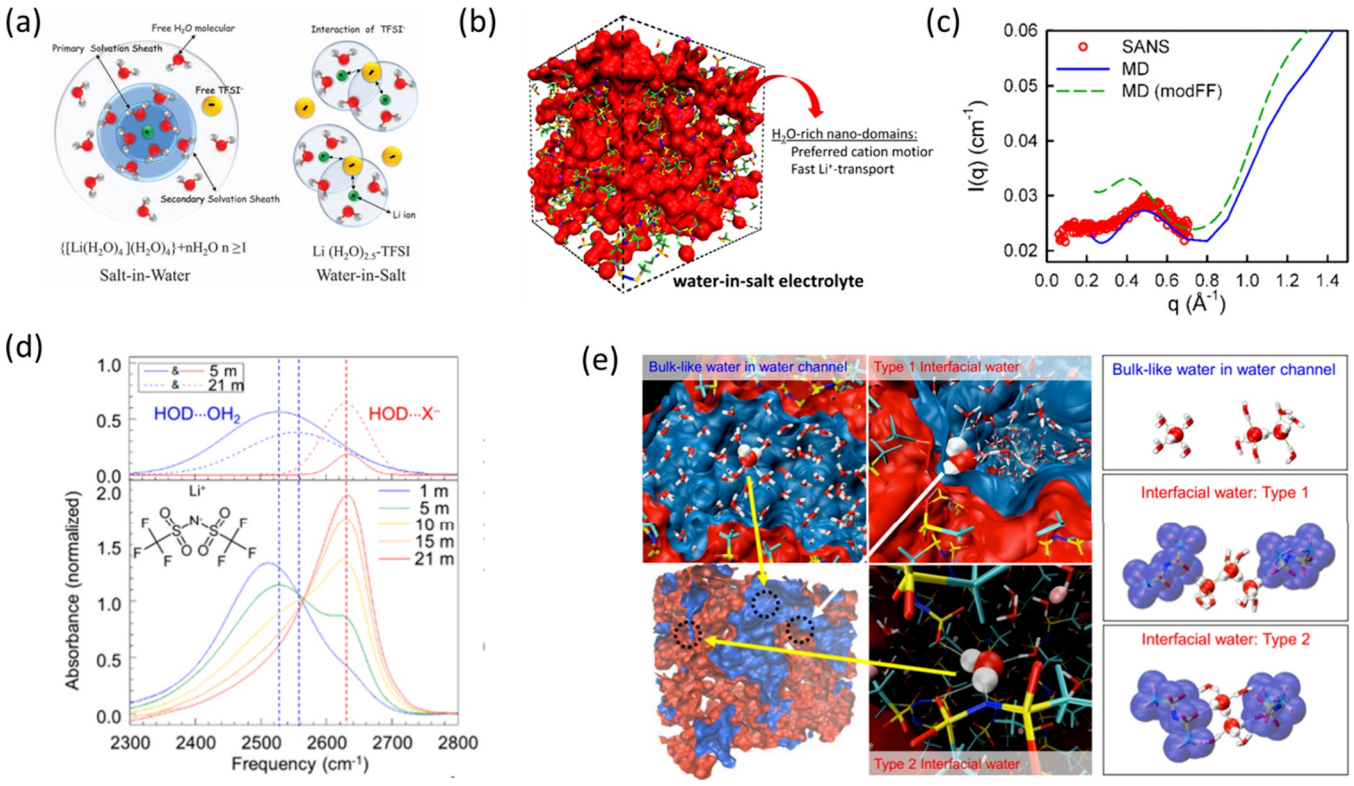

Figure 2. (a) Depiction of the development of the primary solvation sheath of Li^+ in diluted and water-in-salt solutions. Figure reproduced with permission from ref 39. Copyright 2015 American Association for the Advancement of Science. (b) A three-dimensional image captured from molecular dynamics simulations at 298 K, displaying a network of interconnected H_2O molecules in red and TFSI anions represented as a wireframe, in a 21 m LiTFSI–H_2O solution. (c) The structure factor obtained from small-angle neutron scattering (SANS) experiments and molecular dynamics (MD) simulations for a 21 m LiTFSI solution in deuterium oxide (D_2O). Figure reproduced with permission from ref 20. Copyright 2017 American Chemical Society. (d) The infrared (IR) absorption spectra displaying the OD stretch mode of HOD in LiTFSI aqueous solutions (lower panel), accompanied by the outcomes of Gaussian fitting analysis for 5 and 21 m LiTFSI concentrations in aqueous solutions (upper panel). (e) Type-1 interfacial water molecules establish hydrogen bonds with neighboring bulk-like water molecules and $TFSI^-$, while type-2 interfacial water molecules engage in two or more electrostatic interactions with $TFSI^-$. Figure reproduced with permission from ref 21. Copyright 2018 American Chemical Society.

categorized into two families: esters and ethers.[12] The most widely used and successful commercial lithium salt in lithium-ion batteries is $LiPF_6$. Many studies have been conducted to understand the impact of microscopic structures on the physical and chemical characteristics of battery electrolytes;[34−36] however, the microstructures of solvation interactions of ions of commercial liquid electrolytes are still not fully understood.

We conducted a microscopic structure analysis on cyclic EC within cyclic PC and linear carbonate electrolytes, including DMC, EMC, and DEC using SAXS,[38] as shown in Figure 1. The SAXS curves for PC and EC/PC were nearly identical, indicating that the two solutions share the same structure (Figure 1a). However, Figure 1b,c shows that the SAXS curves for EC/EMC and EC/DEC exhibited a noticeable increase in intensity within the q range of 0.02 to 0.5 $Å^{-1}$. When EC dissolves in EMC or DEC, molecular rearrangement occurs because EC and PC are cyclic carbonates, while EMC and DEC are linear carbonates. As a result, some EC molecules may create small clusters in the linear carbonate solvents. The SAXS intensity data of pure EMC were subtracted from the SAXS intensity data of EC/EMC. Only the form factor of the sample appears. Based on the volume distribution, the mean diameter of the nanostructure was estimated to be around 1 nm through data fitting. Furthermore, we investigated the 1 M $LiPF_6$/carbonate electrolytes. The observation of $LiPF_6$ contact ion pairs is limited to the EC/EMC electrolyte and not in EC/PC mixtures, primarily due to the differences in the dielectric constant between EMC and PC.

Ahmadiparidari et al. presented a new chemistry based on a combination of $LiNO_3$, TEGDME, and an ionic liquid that enables LiI (1 M) to lower the charge potential (3.5 V) with a long cycle life of 270 cycles which is used in Li–O_2 batteries.[37] They also used SAXS to investigate the solvation structures. Figure 1d depicts the SAXS data obtained from various samples, including pure IL, TEGDME, IL/TEGDME, and IL/TEGDME with the addition of LiI and $LiNO_3$ salts. No aggregated signals were observed in the case of the pure IL and TEGDME samples. However, aggregate formations of varying sizes were evident for the IL/TEGDME and IL/TEGDME samples with LiI/$LiNO_3$ salts. Specifically, the SAXS curve for IL/TEGDME exhibited a noticeable increase in intensity within the scattering vector, q, ranging from 0.05 to 0.5 $Å^{-1}$ when compared with the IL and TEGDME samples. They employed the spherical model to perform a fitting analysis of the subtracted data within the q range of 0.05–0.5 $Å^{-1}$. By fitting the data with the Lognormal model, represented by the red curve from the form factor of the samples in Figure 1e, they could estimate the nanostructures' average diameter to be approximately 3 nm, as depicted in Figure 1f.

https://doi.org/10.1021/acs.chemmater.3c01648
Chem. Mater. 2023, 35, 9821−9832

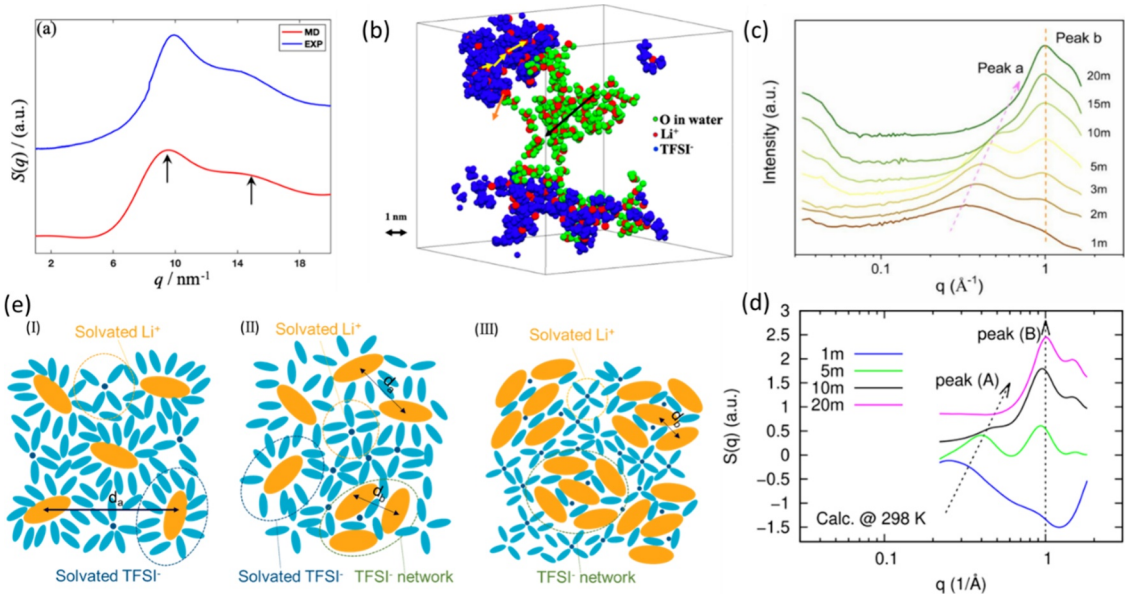

Figure 3. (a) Structure factor calculated using molecular dynamics (MD) simulations (red) and from the SAXS experiment (blue) for a 20 m LiTFSI aqueous electrolyte. (b) Representative snapshot of the largest water and ionic aggregates in 20 m LiTFSI in water. The Li^+ diffusion mechanisms and paths in the different domains are also indicated with arrows. Reprinted with permission under a Creative Commons CC BY 4.0 from ref 40. Copyright 2020 American Chemical Society. (c) SAXS profile of LiTFSI aqueous electrolytes at different concentrations under room temperature. (d) Calculated X-ray structure factor at the low q range as a function of LiTFSI concentration. Ref 25 Copyright 2021 American Chemical Society. (e) Three concentration regimes are divided: (I) low concentration, (II) medium concentration, and (III) high concentration. Figure reproduced with permission from ref 18. Copyright 2021 American Association for the Advancement of Science.

WATER-IN-SALT

The electrolyte concentration significantly influences battery performance, and many studies have investigated the correlation between the electrolyte concentration and the battery's electrochemical performance. Yamada et al. proposed that the high concentration could broaden the electrolyte's electrochemical stability window and make the electrolyte's oxidation potential significantly improve.[28] Wang's group applied this strategy to aqueous LIBs and made significant progress in the performance of aqueous LIBs.[39] They reported a new aqueous electrolyte called "water-in-salt" (WIS), which contains 21 mL of LiTFSI. This aqueous electrolyte has a larger electrochemical stability window, about 3.0 V, which is comparable to the organic electrolytes used in commercial LIBs.

Because of the excellent electrochemical performances of WIS electrolytes, scientists have tried to investigate their solvation structure. In the beginning, Wang's group provided their assumption about the solvation structure of the WIS electrolyte.[39] For the dilute LiTFSI aqueous electrolyte, Li^+ is solvated by water molecules, and $TFSI^-$ remains relatively free. However, for the WIS electrolyte, on average, two TFSI anions exist in each Li^+ primary solvation sheath (Figure 2a). Borodin et al. investigated the ion solvation and transport in LiTFSI aqueous system in a wide concentration range combined with MD simulation and small-angle neutron scattering (SANS),[20] as shown in Figure 2b,c. They found the disproportionation of cation solvation leads to a heterogeneous liquid structure and creates two interpenetrating but dynamics nanodomain networks. The TFSI-rich domain immobilizes the anion movement relatively, and the $Li^+(H_2O)_4$ domain serves as a percolating channel for fast Li^+ transports with a high lithium-transference number. Combining infrared spectroscopy (IR) (Figure 2d) and molecular dynamics (MD) simulation, Cho et al. proved that there are two different kinds of water. One is bulk-like water, which plays the positive role as a medium for lithium-ion transport in ion transport channels within porous anions network; the other is interfacial water, which looks like the lubricant in anion networks[21] (Figure 2e). TFSI anions are mainly responsible for the formation of anion networks, which act as a framework for nanometer water channels.

However, the techniques employed in previous studies, such as NMR,[31,32] Raman,[26−30] and IR spectroscopy,[21,24,25] are only sensitive to the local molecular bonding and orientations and are challenging to capture the whole structure of the forming clusters and aggregates. SAXS provides information about the molecules' size and shape and assemblies from 1 to 150 nm in solution. Using SAXS and MD simulation, our group and Cheng's group observed a heterogeneous structure within the 20 m LiTFSI aqueous electrolyte.[40] Our findings suggest that this heterogeneous structure is responsible for this system's relatively high transference number. Because of the high concentration of the samples, the structure factor shows up. Two peaks at high q can be observed from the SAXS profiles and the MD simulation results agree with the SAXS results, as shown in Figure 3a. This also shows that SAXS data could be the standard to validate the force field in the MD simulation. The simulations demonstrated the existence of networks of negatively charged ion domains and positively charged water domains that permeate the system. While the dynamics of Li^+ within the ion domain exhibit a strong correlation, the movement of Li^+ in the water domain is comparatively unrestricted (Figure 3b). This is because of the low number of anions in the water domain, which results in a weak interion correlation and ultimately leads to a relatively high t_c^+ despite the high viscosity.

Despite many studies examining the structures of highly concentrated LiTFSI aqueous electrolytes, the solvation

https://doi.org/10.1021/acs.chemmater.3c01648
Chem. Mater. 2023, 35, 9821−9832

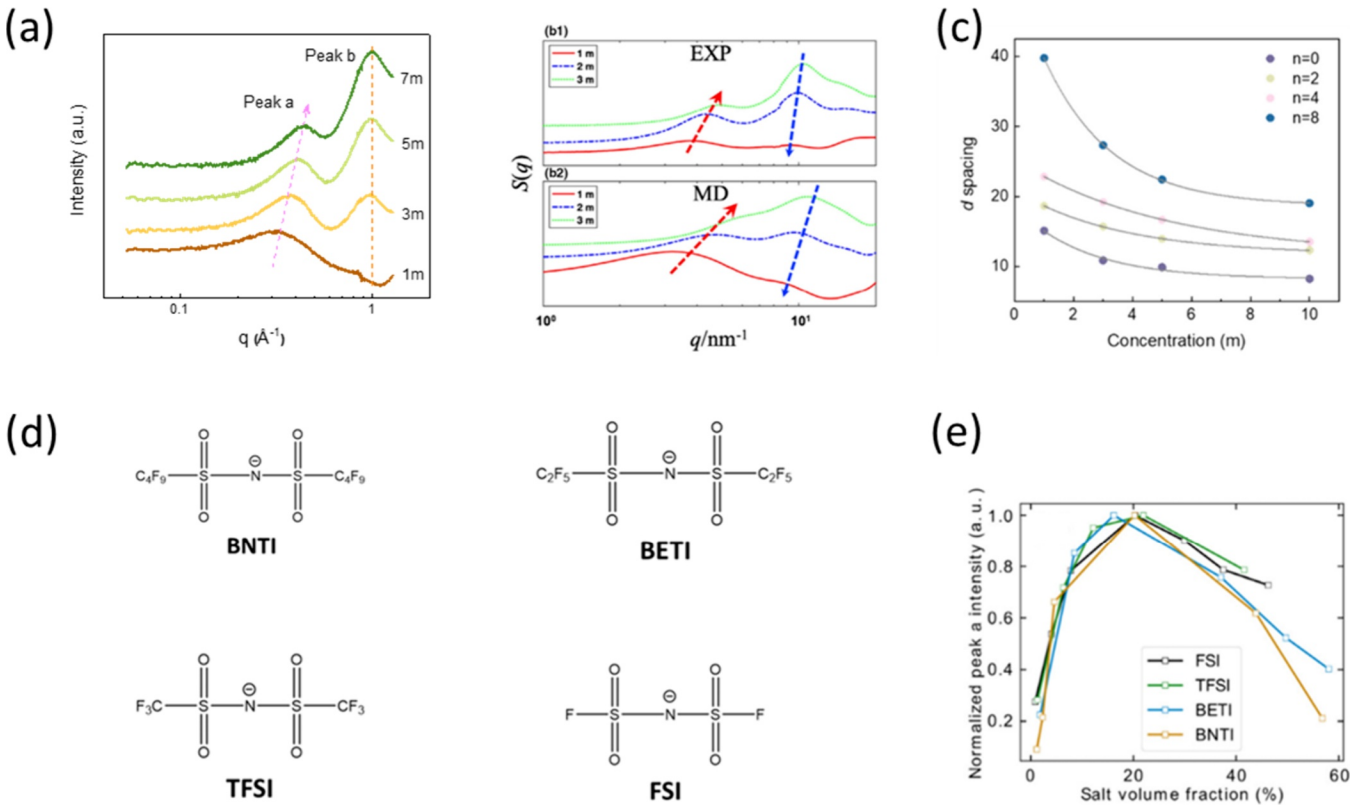

Figure 4. (a) SAXS profile of NaTFSI aqueous solutions with different concentrations at room temperature. Structure factors of the 1, 2, and 3 m aqueous electrolytes. Reprinted with permission under a Creative Commons CC BY 4.0 from ref 18. Copyright 2021 American Association for the Advancement of Science. (b1) are measured using SAXS and (b2) calculated using MD simulation to understand the $Mg(TFSI)_2$ aqueous system. Figure reproduced with permission from ref 46. Copyright 2021 Wiley. (c) Evolution of the correlation *d* spacing with the different concentrations of the four imide-based anions. (d) The chemical formula of FSI, TFSI, BETI, and BNTI. (e) Normalized peak intensity as a function of salt volume fraction. Figure portion (c) and (e) reproduced with permission from ref 19. Copyright 2022 Elsevier.

behaviors under different concentrations remain poorly understood. Our group systematically varied the LiTFSI concentrations and measured them with SAXS at room temperature. From the SAXS profile[18] (Figure 3c), two peaks can be observed; one is named as Peak a in the low *q* part, and the other is marked as Peak b at relative high *q* part, which is at 0.99 Å^{-1}. Peak a represents the $TFSI^-$ solvated structure. Unlike the other papers that ascribed Peak b to the charge-ordering peak, which is usually used for ionic liquid and molten salts,[41,42] we ascribe it to the $TFSI^-$ network that TFSI anions were mainly linked by interfacial water, not cations, which is also consistent with IR results in Figure 2d. The position of Peak b for the NaTFSI solution is found to be identical to that of LiTFSI (Figure 4a). This suggests that the cation (Na^+) does not play a crucial role in determining Peak b's position. If the cation were a significant factor, the peak would have been shifted to a lower *q* value due to the larger radius of Na^+ (1.02 Å) compared to Li^+ (0.69 Å).[43] Therefore, it is evident that alternative $TFSI^-$ structures may contribute to this peak. Two possible structures that could account for this observation are as follows: $TFSI^-$ anions in direct contact with each other; $TFSI^-$ anions connected to water molecules, forming a structure like $TFSI^-\cdots HOH\cdots TFSI^-$. The *d*-spacing between the $TFSI^-$ network is measured to be 6.4 Å, which is larger than the pure TFSI–Li–TFSI distance (5.3 Å).[44] As a result, we can attribute the formation of this peak to the $TFSI^-$ network, likely formed by the bridging of water molecules. The Li^+ is still in the $TFSI^-$ network to keep the electronic equilibrium, but it remains uncertain if it is totally solvated by the water molecules (in the water channel) or connected with $TFSI^-$.

LiTFSI aqueous solutions can be divided into three concentration regimes, as shown in Figure 3e: low, medium, and high concentration. The $TFSI^-$ solvated structure is the primary solvated structure at low concentrations, while the $TFSI^-$ solvated structure and the $TFSI^-$ network coexist as the concentration increases to a medium level. However, the $TFSI^-$ network is the only existing solvation structure at high concentrations. Our experimental SAXS results were further confirmed by Zhang et al. with MD simulations.[25] Comparing Figure 3c and 3d, we can observe that their calculated results matched our SAXS profile very well.[25] They assume that the relatively high Li^+ apparent transference number is because the $TFSI^-$ dynamics decrease more quickly with increasing salt concentration than the Li^+ dynamics due to the formation of $TFSI^-$ networks.[45] They also think that the conduction of Li^+ through the high concentration electrolyte occurs mainly through a hopping mechanism instead of a vehicular mechanism. In the vehicular mechanism, the ion traverses in the proximity of its surrounding solvation shell over a considerable distance. On the other hand, in the exchange or hopping mechanism, the ion undergoes continuous transitions between solvating species or effectively "hops" from one solvating species to another.

We also demonstrate that SAXS technique can be used on other $TFSI^-$-based WIS electrolytes (Figure 4a,b).[18,46] Similar

https://doi.org/10.1021/acs.chemmater.3c01648
Chem. Mater. 2023, 35, 9821−9832

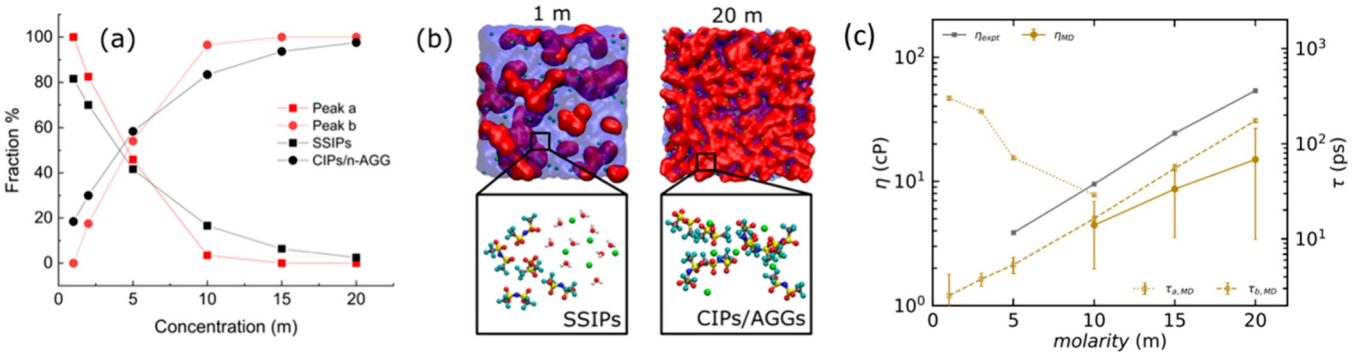

Figure 5. (a) Peak a vs Peak b fraction from SAXS and solvent-separated ion pairs (SSIPs), vs contact ion pairs (CIPs) plus aggregate clusters (AGGs) fraction from MD simulation. (b) MD simulation snapshots show SSIPs, CIPs, and AGGs. (c) Concentration dependence of the viscosities and the average relaxation time associated with Peaks a and b. Reprinted with permission from ref 17. Copyright 2023 American Chemical Society.

to LiTFSI, NaTFSI and $Mg(TFSI)_2$ exhibit two solvation structures, with the $TFSI^-$ solvated structure diminishing as the concentration increases and giving way to the gradual formation of a $TFSI^-$ network. Our group further symmetrically investigates the imide-based lithium salts' aqueous solutions structures. We chose four different symmetric anions (Figure 4d): (bis(fluorosulfonyl)imide (FSI), bis(trifluoromethane sulfonyl)imide (TFSI), bis(pentafluoroethane sulfonyl) imide (BETI), and bis(nonafluorobutane sulfonyl)imide (BNTI)), which have similar parent structures but different lengths of the fluorocarbon chains.[19] We examined the solvation structures and attempted to identify the relationships among *d* spacing, carbon numbers, and concentrations. The carbon numbers of the fluorocarbon chains in the anions and their concentrations influence the *d* spacing of anion-solvated structures. The number of carbons in the fluorocarbon chains has a linear correlation with the *d* spacing, while the concentration has an exponential correlation (Figure 4c). These findings enable prediction of the SAXS/WAXS profiles of aqueous solutions containing the four imide-based lithium salts at any concentration. Molecular dynamics simulations indicate that the formation of anion networks in all imide-based lithium salt solutions begins at around 20% of the salt volume fraction (Figure 4e).

The length scale of solvation structures observed through SAXS differs from the solvation structures reported using Raman at the molecular level, such as solvent-separated ion pairs (SSIPs), contact ion pairs (CIPs), and aggregate clusters (AGGs). Understanding the connection between these solvation structures observed by SAXS and Raman spectroscopy is crucial. It is also important to elucidate water's role in forming the solvation structure of WIS electrolytes.[21] Moreover, the relationship between the viscosity and the solvation structures needs to be clarified. To address the above questions, SAXS, SANS, pair distribution function (PDF), and viscosities were measured for LiTFSI aqueous solutions at different concentrations, and corresponding MD simulations were conducted on the same systems.[17] Our investigation confirmed that the dissimilarities between SAXS and SANS profiles arise mainly from the divergence in X-ray and neutron scattering cross sections of the anions. Our findings indicate that the $TFSI^-$ solvated structure primarily comprises solvent-separated ion pairs, while the $TFSI^-$ network mainly comprises contact ion pairs and aggregates, as shown in Figures 5a,b. SANS confirms that water also forms a cluster at low concentrations. Furthermore, we analyzed the concentration-dependent variations in the viscosities and relaxation times associated with the two solvation structures and found that the viscosity of WIS electrolytes is mainly influenced by the anion network structure (Figure 5c).

SOLVENT-IN-SALT

Although the solubility of inorganic salt in organic solvents is not as excellent as that in water, the wide variety of organic solvents makes the organic electrolyte versatile and rapidly growing in lithium metal batteries.[47] In comparison to traditional dilute organic electrolytes, concentrated electrolytes present several advantages. They contain fewer free-state molecules and exhibit stronger interactions among cations, anions, and solvents. These characteristics result in a range of benefits, including an expanded temperature and potential window, reduced flammability, increased Li^+ transport number, and the formation of a robust solid electrolyte interface (SEI) derived from anions, which exhibits low interfacial resistance.[27,28,48] Moreover, upon surpassing a certain concentration threshold (3−5 M), the concentrated electrolyte undergoes a transformation wherein free solvent molecules become scarce, leading to the emergence of a distinct solvation structure. This new structure plays a crucial role in diminishing the inherent volatility of the concentrated electrolyte. Suo et al. pioneered the solvent-in-salt (SIS) electrolyte by employing concentrated 7 M LiTFSI in DOL/DME (1:1 by volume) in lithium−sulfur (Li−S) batteries.[49] The SIS electrolyte can inhibit the dissolution of soluble lithium polysulfides from the sulfur electrode and suppress lithium dendrite growth. Similarly, only a limited number of free-state solvent molecules coordinate with metal cations from the cathode in LIBs, which helps to suppress the diffusion of those cations into the bulk electrolyte.[50] Because of structure-dependent properties, Raman spectroscopy is the major characterization technique to obtain the SIS structure at the molecular level.[51,52] The introduction of SAXS provides the interactions between cations/anions and electrolyte solvents in the nanoscale.[53]

It should be noted that organic solvents are not as bipolar as the water. They mostly solvate cations not anions. Therefore, they will form solvation structures different from WIS. Amine et al. reported a new class of concentrated siloxane-based electrolytes, which achieved quasi-solid−solid lithiation instead of conventional solid−liquid−solid lithiation in dilute or

https://doi.org/10.1021/acs.chemmater.3c01648
Chem. Mater. 2023, 35, 9821−9832

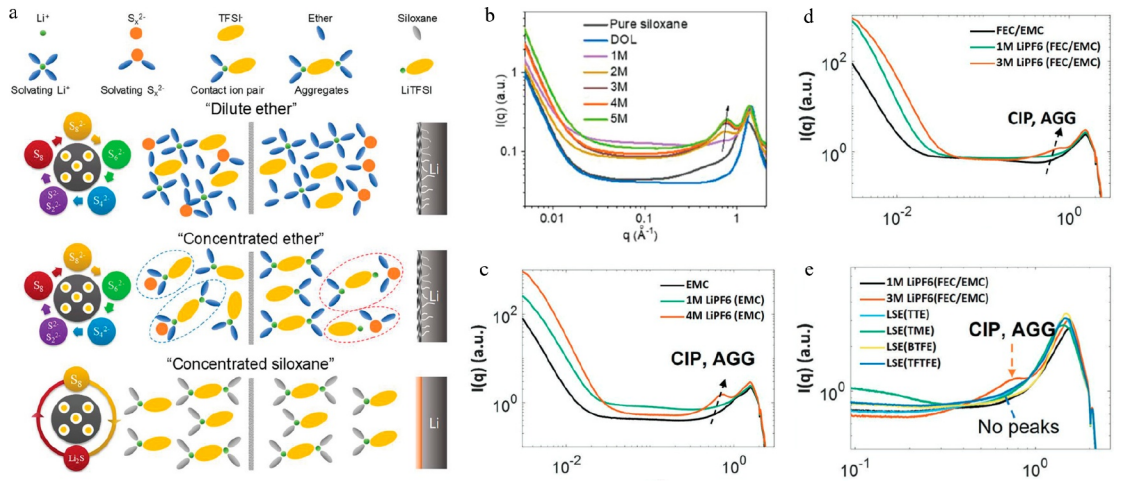

Figure 6. (a) Schematic illustration of sulfur redox chemistry, polysulfide shuttle, and lithium dendrite formation for Li−S batteries in different electrolytes. (b) SAXS data of siloxane-based electrolytes with increased LiTFSI concentration. Reprinted with permission from ref 54. Copyright 2020 Wiley. (c−e) SAXS data of $LiPF_6$ in (ethyl methyl carbonate) EMC, (fluoroethylene carbonate) FEC/EMC, and pure solvents of EMC, FEC/EMC, 1,1,2,2-tetrafluoroethyl-2,2,2,3- tetrafluoropropyl ether (TTE), 1,1,2,2-tetrafluoroethyl methyl ether (TME), bis(2,2,2-trifluoroethyl) ether (BTFE), and 1,1,2,2,-tetrafluoroethyl-2,2,2-trifluoroethyl ether (TFTFE). Figure reproduced with permission from ref 55. Copyright 2022 Wiley.

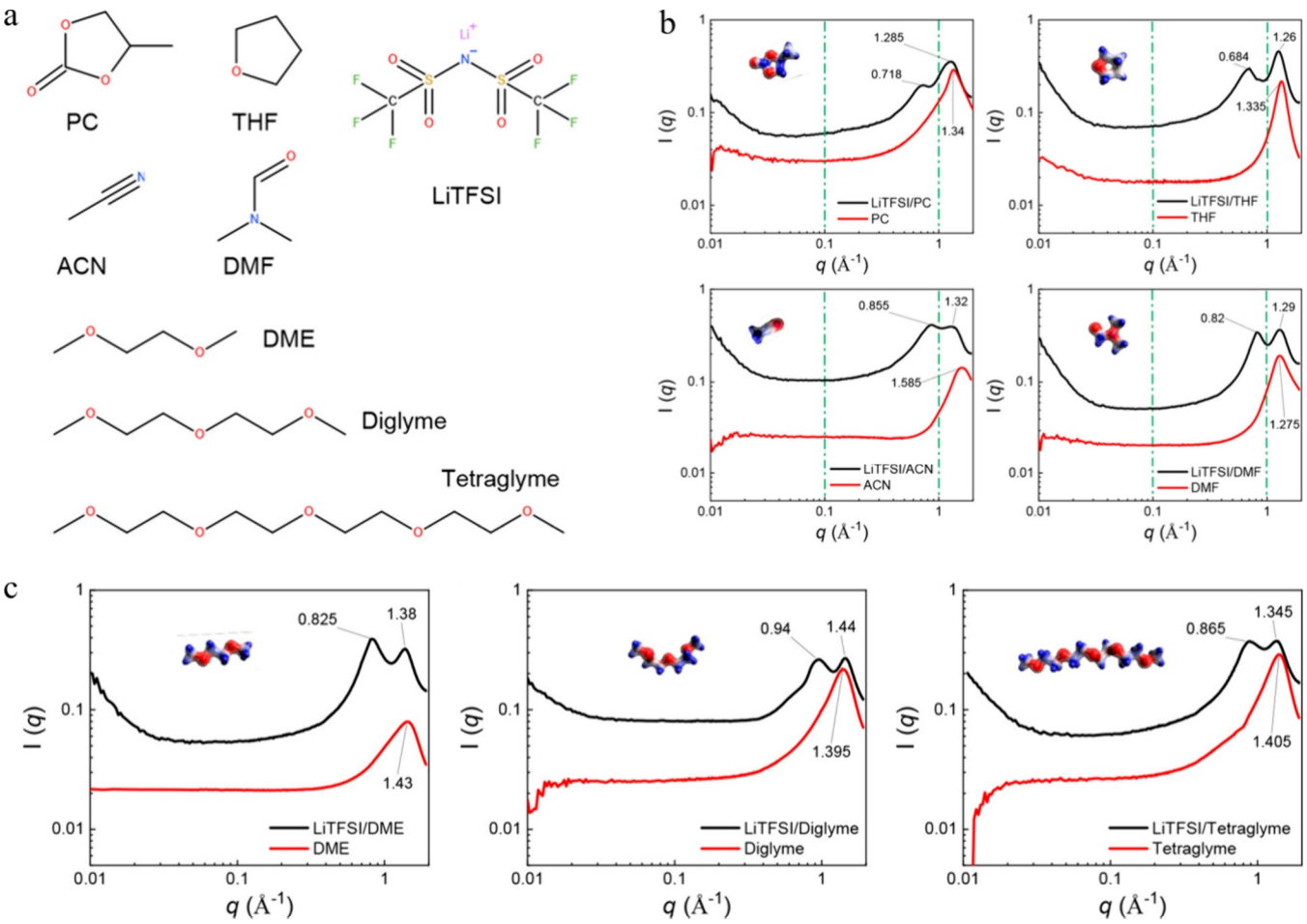

Figure 7. (a) Chemical structures of LiTFSI salt and seven different solvent molecules. (b) Background-corrected SAXS data of saturated electrolytes and their corresponding pure solvents (LiTFSI in PC/THF/ACN/DMF). (c) SAXS of LiTFSI in DME/Diglyme/Tetraglyme. Figure reproduced with permission from ref 56. Copyright 2021 American Chemical Society.

concentrated ether-based electrolytes.[54] Siloxane solvent can effectively regulate the cations/anions and solvents with a solvation-ion-exchange process in the concentrated electrolytes (Figure 6a). SAXS data display a clear intensity increase in the q range from 0.5 to 0.8 $Å^{-1}$ with increased concentration from 1.0 to 5.0 M (Figure 6b), which is ascribed to the formation of

https://doi.org/10.1021/acs.chemmater.3c01648
Chem. Mater. 2023, 35, 9821−9832

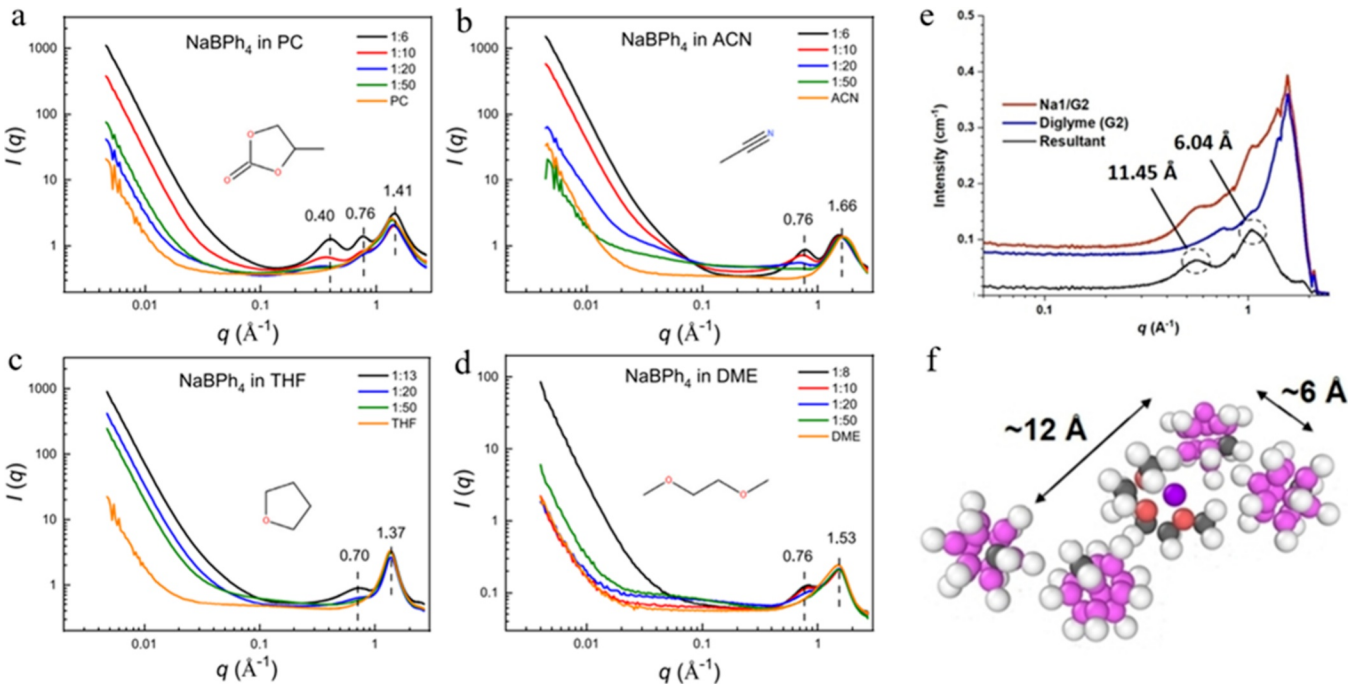

Figure 8. SAXS data of $NaBPh_4$ based solutions with different salt concentrations. (a) $NaBPh_4$ in PC. (b) $NaBPh_4$ in ACN. (c) $NaBPh_4$ in THF. (d) $NaBPh_4$ in DME.[57] Copyright 2022, Elsevier. (e) SAXS data of $Na[HCB_{11}H_{11}]$ in Diglyme. (f) Enlarged image displaying anion−anion separation. Figures reproduced with permission from ref 58. Copyright 2023 Wiley.

CIP, and this is similar to the high q peak observed for the WIS, as shown in Figure 5a,b. As the concentration increases, the peak position shifts to a higher q. Different from the WIS system, there are no low q peaks. The emergence of CIP/AGG clusters in concentrated electrolytes also be reported by Su et al.[55] A broad peak in the q range of 0.5−0.8 $Å^{-1}$ appears in 4 M $LiPF_6$ (EMC) and 3 M $LiPF_6$ (FEC/EMC) (Figure 6c,d), indicating the formation of CIP and/or AGG clusters.[55] The feature peak disappears after adding diluents (Figure 6e), suggesting that the diluent molecules impact the inner solvation structure and alter the size distribution of clusters in the concentrated electrolytes.

Our group conducted a comprehensive SAXS/WAXS study on the solvation structures of LiTFSI-based saturated organic electrolytes.[56] Organic solvents with different molecular shapes/chain lengths and functional groups have been targeted (Figure 7a). As shown in Figure 7b,c, these saturated electrolytes exhibit a similar feature in SAXS/WAXS plots, with a peak at the $-q$ region (0.7−0.9 $Å^{-1}$). Interestingly, the peaks in linear shape molecules (ACN, DMF) are more visible than in ring shape molecules (PC, THF). Moreover, the short chain molecule (DME) is more suitable for forming this peak than a long chain molecule (Diglyme, Tetraglyme).

We found that the steric effect also affects the formation of solvation structures. For instance, the solvation structures of fluorine-free sodium salt sodium tetraphenylborate ($NaBPh_4$) in different organic solvents (PC, ACN, THF, and DME) have been studied.[57] As shown in the SAXS plots of $NaBPh_4$ with different salt concentrations (Figure 8a−d), the prominent peak above 1 $Å^{-1}$ corresponds to the intermolecular distance between the neighboring atoms of different molecules, which is size/shape dependent. As the salt concentration increases from dilute to high, scattering peaks (0.7−0.8 $Å^{-1}$) gradually form with increased intensity, which means the formation of aggregates. Interestingly, one additional characteristic low q peak (0.4 $Å^{-1}$) arises at low concentrations and keeps shifting to high q as the concentration increases were found in $NaBPh_4$ in PC. By combining Raman spectroscopy and MD simulations, we believe it is caused by the short-range stacking of BPh_4−anion clusters. In addition, two peaks were observed in SAXS data of larger $Na[HCB_{11}H_{11}]$ molecules in Diglyme solution, corresponding to anion−anion separation distances of 6.04 and 11.5 Å (Figure 8e,f).[58]

■ RESULTS AND PERSPECTIVES

The complexity of liquid structures, including hydrogen bonding, Coulombic forces, and other ion−molecule interactions, presents more significant challenges than solids or gases. The structure of a solution can be influenced by various factors, including internal molecular shape, polarity, and concentration as well as external environmental conditions, such as temperature and electric fields. As discussed, many useful techniques have been performed in liquid studies; for example, NMR has the capability to identify chemical shifts in particular elements and distinguish the chemical surroundings, which is helpful in analyzing the solvation structure. In addition, the local vibrational mode of the molecules is commonly explored through Raman and infrared spectroscopy. Variations in the bend, twist, or stretch vibrations of free solvent molecules, coordinated solvent molecules, and anions can be detected through specific band shifts in wavenumbers.

However, as new electrolyte systems continue to be proposed, only NMR, Raman, or other technologies which can only offer the local bond or orientation information no longer meet the needs of an in-depth understanding of electrolytes. In order to comprehend how the macroscopic physical behavior (ionic conductivity and viscosity) of a liquid is linked to its structural features (solvation state, cluster size, and arrangement of nanostructures), it is crucial to create a set of analytical tools that can precisely examine these structures

https://doi.org/10.1021/acs.chemmater.3c01648
Chem. Mater. 2023, 35, 9821−9832

Table 1. Summary of Peak Positions and *d* Spacings Derived from SAXS Data from Different Systems

Water-in-Salt					
	Peak Position		*d* Spacing		
	Peak a	Peak b	Peak a	Peak b	Ref
20 m LiTFSI		0.99 $Å^{-1}$		0.628 nm	40
1 to 20 m LiTFSI	Between 0.3 and 0.5 $Å^{-1}$	0.99 $Å^{-1}$	Between 12 and 18 Å	6.35 Å	18
1 to 26 m LiFSI	Between 0.3 and 1 $Å^{-1}$	1.27 $Å^{-1}$	Between 6 and 17 Å	4.95 Å	19
1 to 15 m LiBETI	Between 0.2 and 0.4 $Å^{-1}$	0.90 $Å^{-1}$	Between 13 and 23 Å	6.98 Å	
0.2 to 10 m LiBNTI	Between 0.1 and 0.3 $Å^{-1}$	Between 0.4 and 0.6 $Å^{-1}$	Between 19 and 57 Å	Between 10 and 15 Å	
1 to 3 m $Mg(TFSI)_2$	Between 0.3 and 0.5 $Å^{-1}$	Between 0.8 and 0.9 $Å^{-1}$	Between 12 and 21 Å	Between 7 and 8 Å	46
1 to 7 m NaTFSI	Between 0.3 and 0.4 $Å^{-1}$	0.99 $Å^{-1}$	Between 14 and 19 Å	6.35 Å	18
Solvent-in-Salt					
	Peak Position		*d* Spacing		Ref
1 to 5 M LiTFSI in siloxane electrolytes	between 0.5 and 0.8 $Å^{-1}$		7.8 Å		52
1 and 4 m LiPF6 in EMC	between 0.5 and 0.8 $Å^{-1}$		between 7.9 and 12.6 Å		53
Saturated LiTFSI in PC	0.72 $Å^{-1}$		8.75 Å		54
Saturated LiTFSI in THF	0.68 $Å^{-1}$		9.19 Å		
Saturated LiTFSI in ACN	0.86 $Å^{-1}$		7.35 Å		
Saturated LiTFSI in DMF	0.82 $Å^{-1}$		7.66 Å		
Saturated LiTFSI in DME	0.83 $Å^{-1}$		7.62 Å		
Saturated LiTFSI in diglyme	0.94 $Å^{-1}$		6.68 Å		
Saturated LiTFSI in tetraglyme	0.87 $Å^{-1}$		7.26 Å		
1:6 (molar ratio) $NaBPh_4$ in PC	0.40 and 0.76 $Å^{-1}$		15.7 and 8.26 Å		55
1:6 (molar ratio) $NaBPh_4$ in ACN	0.76 $Å^{-1}$		8.26 Å		
1:13 (molar ratio) $NaBPh_4$ in THF	0.70 $Å^{-1}$		8.98 Å		
1:8 (molar ratio) $NaBPh_4$ in DME	0.76 $Å^{-1}$		8.26 Å		
$Na[HCB_{11}H_{11}]$ in Diglyme	0.55 and 1.04 $Å^{-1}$		11.45 and 6.04 Å		56

from small scale to large scale. SAXS offers a comprehensive overview of the structure that is statistically averaged across the entire sampling region, enabling the determination of critical structural characteristics, such as particle size, shape, porosity, and arrangement. The peak position (q value) and the d spacing in different electrolytes have been summarized in Table 1. It has already been employed in electrolyte research to determine the liquid structure factor and nanostructures, such as solvation, clusters, and aggregates, demonstrating its distinct advantage in this field.

Looking to the future, SAXS can play its unique advantages in the following aspects in the field of electrolytes research. First, by combining SAXS with Raman, FTIR, and NMR techniques, it is possible to explore the solvation structures of electrolytes across several angstroms to hundreds of nanometers (Figure 9). Studies of WIS and $LiPF_6$/EC/EMC electrolytes have shown that they may exhibit heterogeneity. SAXS can confirm the presence of clusters or networks, while Raman, FTIR, and NMR can provide insights into their formation. If the electrolyte is heterogeneous and there are large clusters, we will reconsider the cations' transport mechanism, which is so important in battery engineering. Second, Operando SAXS techniques can take us a step further in unraveling the fundamental mechanisms of liquid dynamics and mass transport under working conditions (temperature, voltage, pressure, etc.), providing crucial and irreplaceable evidence. The development of a new operando setup that combines different techniques (such as X-ray absorption spectroscopy, Raman spectroscopy, etc.) may allow us to observe the bond breaking and making, the large cluster formation and disappearance, and the ionic moving during battery charging and discharging, as shown in Figure 9. There is a paucity of reported in situ/operando SAXS experiments solely focused on investigating the solvation structure of liquid electrolytes related to the main topic of this perspective. Third, SAXS can be used as a standard experimental result to validate the force field use in the MD, which is also a challenge for the MD simulations. With the correct force field, MD simulations can provide more reliable information about the solvation structure and transport property.

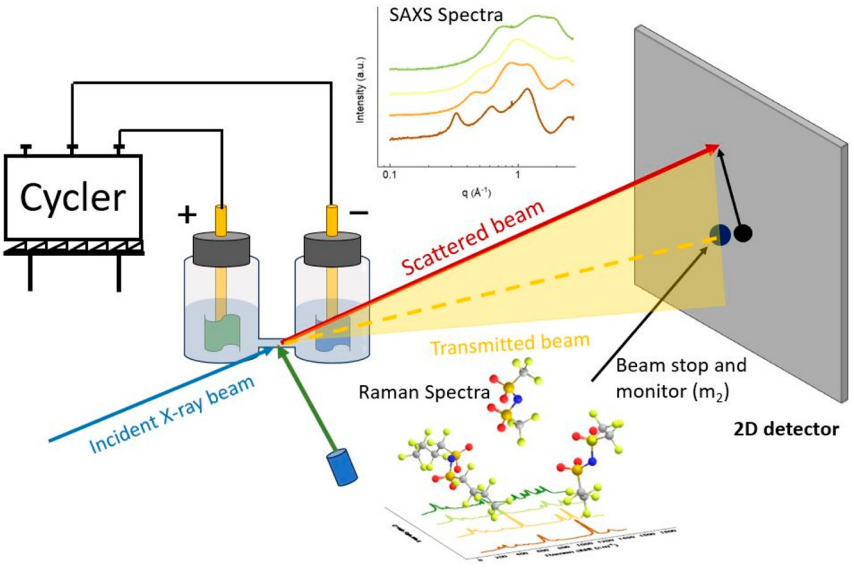

Figure 9. *In situ* SAXS/WAXS/Raman characterization of electrolytes.

https://doi.org/10.1021/acs.chemmater.3c01648
Chem. Mater. 2023, 35, 9821−9832

Regarding particular opportunities for future developments to understand the relationship between solvation structures and properties of electrolytes, we see several significant points to be addressed in the future concerning using SAXS: (1) The impact of beam damage can never be overlooked. Several techniques can be employed to reduce beam "damage", including shortening the exposure time, reducing flux, adding glycerol, and more. However, caution must be exercised when liquid electrolytes are examined, particularly those with high concentrations that employ water as the solvent. In such cases, the use of a flow cell for conducting the study of liquid electrolytes is a wise option. (2) Beyond the in situ transmission SAXS/WAXS, in situ grazing incidence small- and wide-angle X-ray scattering (GISAXS/GIWAXS) could also be a valuable method to revealing electrochemistry. In our group's previous work, we already have confirmed the solvation structure of the liquid electrolyte in the bulk state. *In-situ* GISAXS could potentially serve as a valuable technique for elucidating the solvation structure of electrolytes at the electrode interface during charge and discharge.

AUTHOR INFORMATION

Corresponding Author

Tao Li − *Department of Chemistry and Biochemistry, Northern Illinois University, DeKalb, Illinois 60115, United States; X-ray Science Division, Argonne National Laboratory, Lemont, Illinois 60439, United States; Joint Center for Energy Storage Research, Argonne National Laboratory, Lemont, Illinois 60439, United States;* orcid.org/0000-0002-4913-4486; Email: tli4@niu.edu, taoli@anl.gov

Authors

Xinyi Liu − *Department of Chemistry and Biochemistry, Northern Illinois University, DeKalb, Illinois 60115, United States;* orcid.org/0000-0001-6092-2558

Lingzhe Fang − *Department of Chemistry and Biochemistry, Northern Illinois University, DeKalb, Illinois 60115, United States*

Xingyi Lyu − *Department of Chemistry and Biochemistry, Northern Illinois University, DeKalb, Illinois 60115, United States;* orcid.org/0000-0002-5781-2486

Randall E. Winans − *X-ray Science Division, Argonne National Laboratory, Lemont, Illinois 60439, United States; Joint Center for Energy Storage Research, Argonne National Laboratory, Lemont, Illinois 60439, United States;* orcid.org/0000-0002-7080-7673

Complete contact information is available at: https://pubs.acs.org/10.1021/acs.chemmater.3c01648

Notes

The authors declare no competing financial interest.

Biographies

Xinyi Liu received her master's degree in Chemical Engineering from Wuhan Institute of Technology in 2017. She is currently a Ph.D. candidate under the guidance of Prof. Tao Li at Northern Illinois University; her research is focused on using small-angle X-ray scattering to investigate the solvation structures of the electrolytes.

Lingzhe Fang is currently a Ph.D. candidate under the supervision of Prof. Tao Li in the Department of Chemistry and Biochemistry at Northern Illinois University. He obtained his M.S. degree in 2019 in material science from Nanjing University of Science and Technology in China. His research focuses on the single-atom catalysts for the energy conversion area and battery electrolyte study.

Xingyi Lyu obtained a bachelor's degree in Chemical Engineering from Northeast Forestry University (Harbin, China) in 2018, followed by a Master of Science degree in Chemical Engineering from the University of Florida in 2020. Currently, under the guidance of Professor Tao Li at Northern Illinois University, his research focuses on the electrolyte structure and the development of in situ synchrotron X-ray techniques.Xingyi Lyu obtained a bachelor's degree in Chemical Engineering from Northeast Forestry University (Harbin, China) in 2018, followed by a Master of Science degree in Chemical Engineering from the University of Florida in 2020. Currently, under the guidance of Professor Tao Li at Northern Illinois University, his research focuses on the electrolyte structure and the development of in situ synchrotron X-ray techniques.

Randall E. Winans is a Senior Scientist in the X-ray Science Division at Argonne National Laboratory. He has developed in situ X-ray techniques to understand the fundamental chemistry of complex disordered solid and solution systems, such as energy storage materials, catalysts, soot, heavy petroleum, oil shale, and carbons. Chemistry is combined with characterization techniques, including mass spectrometry, IR, and X-ray scattering and spectroscopy. IR and MS are used simultaneously with X-ray techniques.

Tao Li is an associate professor in the Department of Chemistry and Biochemistry at Northern Illinois University and holds a joint scientist position at the Advanced Photon Source at Argonne National Lab. His research interests focus on using advanced X-ray techniques to study nanoparticle self-assembly and energy materials, including catalyst and battery. Dr. Li completed his Ph.D. in the Department of Chemistry and Biochemistry at the University of South Carolina—Columbia in 2009. In 2022, he was awarded ACS ENFL Emerging Research Award and selected to be the class of 2022 Illinois Science & Technology Coalition Researchers to know.

ACKNOWLEDGMENTS

This work was supported as part of the Joint Center for Energy Storage Research, an Energy Innovation Hub funded by the U.S. Department of Energy, Office of Science, Basic Energy Sciences. This research used resources of the Advanced Photon Source, a U.S. Department of Energy (DOE) Office of Science User Facility operated for the DOE Office of Science by Argonne National Laboratory under Contract No. AC02-06CH11357. T. Li is thankful for the support by U.S. National Science Foundation (Grant Nos. 2208972, 2120559, and 2323117). This work was supported as part of the Center for Steel Electrification by Electrosynthesis (C-STEEL), an Energy Earthshot Research Center funded by the U.S. Department of Energy, Office of Science, Basic Energy Sciences (BES) and Advanced Scientific Computing Research (ASCR).

REFERENCES

(1) Manthiram, A. An Outlook on Lithium Ion Battery Technology. *ACS Cent Sci.* **2017**, *3* (10), 1063−1069.

(2) Wang, C. Y.; Liu, T.; Yang, X. G.; Ge, S.; Stanley, N. V.; Rountree, E. S.; Leng, Y.; McCarthy, B. D. Fast charging of energy-dense lithium-ion batteries. *Nature* **2022**, *611* (7936), 485−490.

(3) Li, M.; Lu, J.; Chen, Z.; Amine, K. 30 Years of Lithium-Ion Batteries. *Adv. Mater.* **2018**, *30*, 1800561.

(4) Zeng, X.; Li, J.; Singh, N. Recycling of Spent Lithium-Ion Battery: A Critical Review. *Critical Reviews in Environmental Science and Technology* **2014**, *44* (10), 1129−1165.

(5) Raza, W.; Ali, F.; Raza, N.; Luo, Y.; Kim, K.-H.; Yang, J.; Kumar, S.; Mehmood, A.; Kwon, E. E. Recent advancements in supercapacitor technology. *Nano Energy* **2018**, *52*, 441−473.
(6) Frackowiak, E. Carbon materials for supercapacitor application. *Physical chemistry chemical physics* **2007**, *9* (15), 1774−1785.
(7) Poonam; Sharma, K.; Arora, A.; Tripathi, S.K. Review of supercapacitors: Materials and devices. *Journal of Energy Storage* **2019**, *21*, 801−825.
(8) Şahin, M. E.; Blaabjerg, F.; Sangwongwanich, A. A comprehensive review on supercapacitor applications and developments. *Energies* **2022**, *15* (3), 674.
(9) Yu, Z.; Tetard, L.; Zhai, L.; Thomas, J. Supercapacitor electrode materials: nanostructures from 0 to 3 dimensions. *Energy Environ. Sci.* **2015**, *8* (3), 702−730.
(10) Mekhilef, S.; Saidur, R.; Safari, A. Comparative study of different fuel cell technologies. *Renewable and Sustainable Energy Reviews* **2012**, *16* (1), 981−989.
(11) Tarascon, J.-M.; Armand, M. Issues and challenges facing rechargeable lithium batteries. *Nature* **2001**, *414* (15), 359.
(12) Meng, Y. S.; Srinivasan, V.; Xu, K. Designing better electrolytes. *Science* **2022**, *378* (6624), No. eabq3750.
(13) Dougassa, Y. R.; Jacquemin, J.; El Ouatani, L.; Tessier, C.; Anouti, M. Viscosity and carbon dioxide solubility for LiPF6, LiTFSI, and LiFAP in alkyl carbonates: lithium salt nature and concentration effect. *J. Phys. Chem. B* **2014**, *118* (14), 3973−3980.
(14) Tatara, R.; Yu, Y.; Karayaylali, P.; Chan, A. K.; Zhang, Y.; Jung, R.; Maglia, F.; Giordano, L.; Shao-Horn, Y. Enhanced cycling performance of Ni-rich positive electrodes (NMC) in Li-ion batteries by reducing electrolyte free-solvent activity. *ACS Appl. Mater. Interfaces* **2019**, *11* (38), 34973−34988.
(15) Zheng, J.; Lochala, J. A.; Kwok, A.; Deng, Z. D.; Xiao, J. Research progress towards understanding the unique interfaces between concentrated electrolytes and electrodes for energy storage applications. *Advanced Science* **2017**, *4* (8), 1700032.
(16) Qian, K.; Winans, R. E.; Li, T. Insights into the Nanostructure, Solvation, and Dynamics of Liquid Electrolytes through Small-Angle X-Ray Scattering. *Adv. Energy Mater.* **2021**, *11*, 2002821.
(17) Liu, X.; Lee, S.-C.; Seifert, S.; He, L.; Do, C.; Winans, R. E.; Kwon, G.; Z, Y.; Li, T. Revealing the Correlation between the Solvation Structures and the Transport Properties of Water-in-Salt Electrolytes. *Chem. Mater.* **2023**, *35* (5), 2088−2094.
(18) Liu, X.; Yu, Z.; Sarnello, E.; Qian, K.; Seifert, S.; Winans, R. E.; Cheng, L.; Li, T. Microscopic Understanding of the Ionic Networks of "Water-in-Salt" Electrolytes. *Energy Material Advances* **2021**, DOI: 10.34133/2021/7368420.
(19) Liu, X.; Lee, S.-C.; Seifer, S.; Winans, R. E.; Cheng, L.; Z, Y.; Li, T. Insight into the nanostructure of "water in salt" solutions: A SAXS/WAXS study on imide-based lithium salts aqueous solutions. *Energy Storage Materials* **2022**, *45*, 696−703.
(20) Borodin, O.; Suo, L.; Gobet, M.; Ren, X.; Wang, F.; Faraone, A.; Peng, J.; Olguin, M.; Schroeder, M.; Ding, M. S.; Gobrogge, E.; von Wald Cresce, A.; Munoz, S.; Dura, J. A.; Greenbaum, S.; Wang, C.; Xu, K. Liquid Structure with Nano-Heterogeneity Promotes Cationic Transport in Concentrated Electrolytes. *ACS Nano* **2017**, *11* (10), 10462−10471.
(21) Lim, J.; Park, K.; Lee, H.; Kim, J.; Kwak, K.; Cho, M. Nanometric Water Channels in Water-in-Salt Lithium Ion Battery Electrolyte. *J. Am. Chem. Soc.* **2018**, *140* (46), 15661−15667.
(22) Han, M.; Zhang, R.; Gewirth, A. A.; Espinosa-Marzal, R. M. Nanoheterogeneity of LiTFSI Solutions Transitions Close to a Surface and with Concentration. *Nano Lett.* **2021**, *21* (5), 2304−2309.
(23) McEldrew, M.; Goodwin, Z. A. H.; Bi, S.; Kornyshev, A. A.; Bazant, M. Z. Ion Clusters and Networks in Water-in-Salt Electrolytes. *J. Electrochem. Soc.* **2021**, *168* (5), 050514.
(24) Xie, J.; Liang, Z.; Lu, Y. C. Molecular crowding electrolytes for high-voltage aqueous batteries. *Nat. Mater.* **2020**, *19* (9), 1006−1011.
(25) Zhang, Y.; Lewis, N. H. C.; Mars, J.; Wan, G.; Weadock, N. J.; Takacs, C. J.; Lukatskaya, M. R.; Steinruck, H. G.; Toney, M. F.; Tokmakoff, A.; Maginn, E. J. Water-in-Salt LiTFSI Aqueous Electrolytes. 1. Liquid Structure from Combined Molecular Dynamics Simulation and Experimental Studies. *J. Phys. Chem. B* **2021**, *125* (17), 4501−4513.
(26) Yamada, Y.; Usui, K.; Sodeyama, K.; Ko, S.; Tateyama, Y.; Yamada, A. Hydrate-melt electrolytes for high-energy-density aqueous batteries. *Nature Energy* **2016**, *1* (10), 16129.
(27) Wang, J.; Yamada, Y.; Sodeyama, K.; Chiang, C. H.; Tateyama, Y.; Yamada, A. Superconcentrated electrolytes for a high-voltage lithium-ion battery. *Nat. Commun.* **2016**, *7*, 12032.
(28) Yamada, Y.; Furukawa, K.; Sodeyama, K.; Kikuchi, K.; Yaegashi, M.; Tateyama, Y.; Yamada, A. Unusual stability of acetonitrile-based superconcentrated electrolytes for fast-charging lithium-ion batteries. *J. Am. Chem. Soc.* **2014**, *136* (13), 5039−5046.
(29) Suo, L.; Oh, D.; Lin, Y.; Zhuo, Z.; Borodin, O.; Gao, T.; Wang, F.; Kushima, A.; Wang, Z.; Kim, H. C.; Qi, Y.; Yang, W.; Pan, F.; Li, J.; Xu, K.; Wang, C. How Solid-Electrolyte Interphase Forms in Aqueous Electrolytes. *J. Am. Chem. Soc.* **2017**, *139* (51), 18670−18680.
(30) Dou, Q.; Lei, S.; Wang, D.-W.; Zhang, Q.; Xiao, D.; Guo, H.; Wang, A.; Yang, H.; Li, Y.; Shi, S.; Yan, X. Safe and high-rate supercapacitors based on an "acetonitrile/water in salt" hybrid electrolyte. *Energy Environ. Sci.* **2018**, *11* (11), 3212−3219.
(31) Guo, Y.; Terban, M. W.; Moudrakovski, I.; Münchinger, A.; Dinnebier, R. E.; Popovic, J.; Maier, J. Ion transport in semi-solid in-salt electrolytes: LiTFSI-H_2O as a model system. *Journal of Materials Chemistry A* **2023**, *11* (7), 3427−3436.
(32) Dubouis, N.; Park, C.; Deschamps, M.; Abdelghani-Idrissi, S.; Kanduč, M.; Colin, A.; Salanne, M.; Dzubiella, J.; Grimaud, A.; Rotenberg, B. Chasing aqueous biphasic systems from simple salts by exploring the LiTFSI/LiCl/H2O phase diagram. *ACS central science* **2019**, *5* (4), 640−643.
(33) Li, T.; Senesi, A. J.; Lee, B. Small Angle X-ray Scattering for Nanoparticle Research. *Chem. Rev.* **2016**, *116* (18), 11128−11180.
(34) Valøen, L. O.; Reimers, J. N. Transport properties of LiPF6-based Li-ion battery electrolytes. *J. Electrochem. Soc.* **2005**, *152* (5), A882.
(35) Dahbi, M.; Ghamouss, F.; Tran-Van, F.; Lemordant, D.; Anouti, M. Comparative study of EC/DMC LiTFSI and LiPF6 electrolytes for electrochemical storage. *J. Power Sources* **2011**, *196* (22), 9743−9750.
(36) Campion, C. L.; Li, W.; Lucht, B. L. Thermal decomposition of $LiPF_6$-based electrolytes for lithium-ion batteries. *J. Electrochem. Soc.* **2005**, *152* (12), A2327.
(37) Ahmadiparidari, A.; Fuladi, S.; Majidi, L.; Plunkett, S.; Sarnello, E.; Gholivand, H.; Hemmat, Z.; Rastegar, S.; Misal, S. N.; Jimenez, N.; Redfern, P. C.; Wen, J.; Li, T.; Ngo, A. T.; Khalili-Araghi, F.; Curtiss, L. A.; Salehi-Khojin, A. Enhancing the performance of lithium oxygen batteries through combining redox mediating salts with a lithium protecting salt. *J. Power Sources* **2021**, *491*, 229506.
(38) Feng, Z.; Sarnello, E.; Li, T.; Cheng, L. Communication—Microscopic View of the Ethylene Carbonate Based Lithium-Ion Battery Electrolyte by X-ray Scattering. *J. Electrochem. Soc.* **2019**, *166* (2), A47−A49.
(39) Suo, L.; Borodin, O.; Gao, T.; Olguin, M.; Ho, J.; Fan, X.; Luo, C.; Wang, C.; Xu, K. Water-in-salt" electrolyte enables high-voltage aqueous lithium-ion chemistries. *Science* **2015**, *350* (6263), 938.
(40) Yu, Z.; Curtiss, L. A.; Winans, R. E.; Zhang, Y.; Li, T.; Cheng, L. Asymmetric Composition of Ionic Aggregates and the Origin of High Correlated Transference Number in Water-in-Salt Electrolytes. *J. Phys. Chem. Lett.* **2020**, *11* (4), 1276−1281.
(41) Perera, A. Charge ordering and scattering pre-peaks in ionic liquids and alcohols. *Phys. Chem. Chem. Phys.* **2017**, *19* (2), 1062−1073.
(42) Bhargava, B. L.; Klein, M. L.; Balasubramanian, S. Structural correlations and charge ordering in a room-temperature ionic liquid. *ChemPhysChem* **2008**, *9* (1), 67−70.

(43) Xiong, Y.; Zhou, J.; Lu, P.; Yin, J.; Wang, Y.; Fan, Z. Electrochemical lithium extraction from aqueous sources. *Matter* **2022**, *5* (6), 1760−1791.
(44) Shimizu, K.; Freitas, A. A.; Atkin, R.; Warr, G. G.; FitzGerald, P. A.; Doi, H.; Saito, S.; Ueno, K.; Umebayashi, Y.; Watanabe, M.; Canongia Lopes, J. N. Structural and aggregate analyses of (Li salt + glyme) mixtures: the complex nature of solvate ionic liquids. *Phys. Chem. Chem. Phys.* **2015**, *17* (34), 22321−22335.
(45) Zhang, Y.; Maginn, E. J. Water-In-Salt LiTFSI Aqueous Electrolytes (2): Transport Properties and Li(+) Dynamics Based on Molecular Dynamics Simulations. *J. Phys. Chem. B* **2021**, *125* (48), 13246−13254.
(46) Yu, Z.; Juran, T. R.; Liu, X.; Han, K. S.; Wang, H.; Mueller, K. T.; Ma, L.; Xu, K.; Li, T.; Curtiss, L. A.; Cheng, L. Solvation Structure and Dynamics of $Mg(TFSI)_2$ Aqueous Electrolyte. *Energy & Environmental Materials* **2022**, *5* (1), 295−304.
(47) Azov, V. A.; Egorova, K. S.; Seitkalieva, M. M.; Kashin, A. S.; Ananikov, V. P. "Solvent-in-salt" systems for design of new materials in chemistry, biology and energy research. *Chem. Soc. Rev.* **2018**, *47* (4), 1250−1284.
(48) Qian, J.; Henderson, W. A.; Xu, W.; Bhattacharya, P.; Engelhard, M.; Borodin, O.; Zhang, J. G. High rate and stable cycling of lithium metal anode. *Nat. Commun.* **2015**, *6*, 6362.
(49) Suo, L.; Hu, Y. S.; Li, H.; Armand, M.; Chen, L. A new class of Solvent-in-Salt electrolyte for high-energy rechargeable metallic lithium batteries. *Nat. Commun.* **2013**, *4*, 1481.
(50) Yamada, Y.; Wang, J.; Ko, S.; Watanabe, E.; Yamada, A. Advances and issues in developing salt-concentrated battery electrolytes. *Nature Energy* **2019**, *4* (4), 269−280.
(51) Jeong, S.-K.; Seo, H.-Y.; Kim, D.-H.; Han, H.-K.; Kim, J.-G.; Lee, Y. B.; Iriyama, Y.; Abe, T.; Ogumi, Z. Suppression of dendritic lithium formation by using concentrated electrolyte solutions. *Electrochem. Commun.* **2008**, *10* (4), 635−638.
(52) Yamada, Y.; Yaegashi, M.; Abe, T.; Yamada, A. A superconcentrated ether electrolyte for fast-charging Li-ion batteries. *Chem. Commun. (Camb)* **2013**, *49* (95), 11194−11206.
(53) Qian, K.; Winans, R. E.; Li, T. Insights into the Nanostructure, Solvation, and Dynamics of Liquid Electrolytes through Small-Angle X-Ray Scattering. *Adv. Energy Mater.* **2021**, *11*, 2002821.
(54) Amine, R.; Liu, J.; Acznik, I.; Sheng, T.; Lota, K.; Sun, H.; Sun, C. J.; Fic, K.; Zuo, X.; Ren, Y.; Ei-Hady, D. A.; Alshitari, W.; Al-Bogami, A. S.; Chen, Z.; Amine, K.; Xu, G. L. Regulating the Hidden Solvation-Ion-Exchange in Concentrated Electrolytes for Stable and Safe Lithium Metal Batteries. *Adv. Energy Mater.* **2020**, *10* (25), 2000901.
(55) Su, L.; Zhao, X.; Yi, M.; Charalambous, H.; Celio, H.; Liu, Y.; Manthiram, A. Uncovering the Solvation Structure of $LiPF_6$-Based Localized Saturated Electrolytes and Their Effect on $LiNiO_2$-Based Lithium-Metal Batteries. *Adv. Energy Mater.* **2022**, *12* (36), 2201911.
(56) Qian, K.; Seifert, S.; Winans, R. E.; Li, T. Understanding Solvation Behavior of the Saturated Electrolytes with Small/Wide-Angle X-ray Scattering and Raman Spectroscopy. *Energy Fuels* **2021**, *35* (23), 19849−19855.
(57) Qian, K.; Yu, Z.; Liu, Y.; Gosztola, D. J.; Winans, R. E.; Cheng, L.; Li, T. Understanding fluorine-free electrolytes via small-angle X-ray scattering. *Journal of Energy Chemistry* **2022**, *70*, 340−346.
(58) Tomich, A. W.; Park, J.; Son, S. B.; Kamphaus, E. P.; Lyu, X.; Dogan, F.; Carta, V.; Gim, J.; Li, T.; Cheng, L.; Lee, E.; Lavallo, V.; Johnson, C. S. A Carboranyl Electrolyte Enabling Highly Reversible Sodium Metal Anodes via a "Fluorine-Free" SEI. *Angew. Chem., Int. Ed. Engl.* **2022**, *61* (51), No. e202208158.

https://doi.org/10.1021/acs.chemmater.3c01648
Chem. Mater. 2023, 35, 9821−9832